Mitochondria dysfunction is one of the causes of diclofenac toxicity in the green alga *Chlamydomonas reinhardtii*

Darya Harshkova[1], Elżbieta Zielińska[1], Magdalena Narajczyk[2], Małgorzata Kapusta[2] and Anna Aksmann[1*]

[1] Department of Plant Experimental Biology and Biotechnology, Faculty of Biology, University of Gdansk, Wita Stwosza 59, 80-308 Gdansk, Poland
[2] Bioimaging Laboratory, Faculty of Biology, University of Gdansk, Wita Stwosza 59, 80-308 Gdansk, Poland

Corresponding Author:
Anna Aksmann[1]
Department of Plant Experimental Biology and Biotechnology, Faculty of Biology, University of Gdansk, Wita Stwosza 59, 80-308 Gdansk, Poland
Email address: anna.aksmann@ug.edu.pl

Abstract

Background. Non-steroidal anti-inflammatory drugs (NSAIDs), such as diclofenac (DCF), form a significant group of environmental contaminants. When the toxic effects of DCF on plants are analyzed, authors often focus on photosynthesis, while mitochondrial respiration is usually overlooked. Therefore, an in vivo investigation of plant mitochondria functioning under DCF treatment is needed. In the present work, we decided to use the green alga Chlamydomonas reinhardtii as a model organism.

Methods.
Synchronous cultures of *Chlamydomonas reinhardtii* strain CC-1690 were treated with DCF at a concentration of 135.5 mg· L^{-1}, corresponding to the toxicological value EC50/24. To assess the effects of short-term exposure to DCF on mitochondrial activity, oxygen consumption rate, mitochondrial membrane potential (MMP) and mitochondrial reactive oxygen species (mtROS) production were analyzed. To inhibit cytochrome *c* oxidase or alternative oxidase activity, potassium cyanide (KCN) or salicylhydroxamic acid (SHAM) were used, respectively. Moreover, the cell's structure organization was analyzed using confocal microscopy and transmission electron microscopy.

Results. The results indicate that short-term exposure to DCF leads to an increase in oxygen consumption rate, accompanied by low MMP and reduced mtROS production by the cells in the treated populations as compared to control ones. These observations suggest an uncoupling of oxidative phosphorylation due to the disruption of mitochondrial membranes, which is consistent with the malformations in mitochondrial structures observed in electron micrographs, such as

40 elongation, irregular forms, and degraded cristae, potentially indicating mitochondrial hyper-
41 fission. The assumption about non-specific DCF action is further supported by comparing
42 mitochondrial parameters in DCF-treated cells to the same parameters in cells treated with
43 selective respiratory blockers: no similarities were found between the experimental variants.
44 **Conclusions.** The results obtained in this work suggest that DCF strongly affects this fraction of
45 cells, that have some developmental or metabolic dysfunctions, while more vital cells are
46 affected only slightly, as it was already indicated in literature. In the cells suffering from DCF
47 treatment, the drug influence on mitochondria functioning in a non-specific way, destroying the
48 structure of mitochondrial membranes. This primary effect led to the uncoupling of oxidative
49 phosphorylation. It can be assumed that mitochondrial dysfunction is an important factor in DCF
50 phytotoxicity. Because studies of the effects of NSAIDs on the functioning of plant mitochondria
51 are relatively scarce, the present work is an important contribution to the elucidation of the
52 mechanism of NSAID toxicity toward non-target plant organisms.
53
54 **Introduction**
55   Non-steroidal anti-inflammatory drugs (NSAIDs) have become a significant group of
56 environmental contaminants in water bodies (Mulkiewicz et al., 2021; Ortúzar et al., 2022).
57 Diclofenac (DCF) is one of the most commonly detected pharmaceuticals in water samples
58 worldwide (Ortúzar et al., 2022). DCF and other NSAIDs were designed as drugs for humans
59 and animals, but their biological effects on non-target organisms, including higher plants and
60 algae, are attracting increasing attention (He et al., 2017; Ortúzar et al., 2022). Nevertheless,
61 precise ecotoxicological information is insufficient.
62   One of the consequences of plant cells' exposure to anthropogenic contaminants, among
63 them pharmaceuticals, is the disruption of cell metabolism and induction of oxidative stress
64 (Schmidt & Redshaw, 2015; He et al., 2017; Hejna, Kapuścińska & Aksmann, 2022). When the
65 toxic effects of DCF on plants are analyzed, authors often focus on the most distinctive
66 biomarkers like photosynthetic efficiency parameters (Copolovici et al., 2017; Majewska et al.,
67 2018, 2021; Hájková et al., 2019; Svobodníková et al., 2020), while another very important
68 process, mitochondrial respiration, is usually overlooked. Bearing in mind that chloroplast-
69 mitochondrion interaction plays an important role in general cell metabolism, as well as in stress
70 tolerance (Van Aken et al., 2009), investigation of mitochondria functioning under DCF
71 treatment is of special interest. The problem is even more interesting because the respiratory
72 electron transport chain functions analogously to the photosynthetic electron transport chain, and
73 there is a lot of evidence that the latter is disrupted under DCF treatment (Kummerová et al.,
74 2016; Hájková et al., 2019; Ben Ouada et al., 2019). Thus, it is likely that not only chloroplasts
75 but also plant mitochondria are susceptible to this drug. This assumption is supported by the
76 observations that DCF causes changes in the functioning of mitochondria in animal cells, such as
77 inhibition of mitochondrial complex III, decrease of mitochondrial membrane potential, increase
78 of the *Bax*, *cytochrome c*, *cas-3*, *cas-8* and *p53* expression at gene transcription level (Ghosh et
79 al., 2016; Darendelioglu, 2020) and by our preliminary observations of changes in mitochondrial

80   membrane potential (MMP) in DCF-treated cells of the green alga *Chlamydomonas reinhardtii*
81   (Harshkova, Zielińska & Aksmann, 2019). The value of MMP, generated by the proton pumps
82   (complexes I, III and IV) may provide some clues to the mitochondria's ability to produce ATP
83   (Zorova et al., 2018). MMP plays an important role also in mitochondrial ion transport (Zorova
84   et al., 2018) and in the regulation of metabolic processes. The MMP value is relatively stable
85   under homeostasis, its change (decrease or increase) could serve as valuable indicator of
86   substance toxicity and the physiological response to stress in unicellular plant organisms.
87   The mitochondrial inner membrane of green algae and plants contains a standard
88   oxidative phosphorylation system with electron transport chain (ETC) complexes (complexes I–
89   IV) and ATP synthase (often named complex V) (Møller, Rasmusson & Van Aken, 2021).
90   However, the existence of an alternative route of electron transport in plant mitochondria,
91   especially the presence of cyanide-resistant alternative oxidase (AOX) (Møller, Rasmusson &
92   Van Aken, 2021), makes investigations of plant mitochondria relatively complicated. On the one
93   hand, the presence of AOX forms a branch in the ETC, partitioning electrons between the
94   cytochrome *c* pathway and the AOX pathway. The consequence of high AOX activity is a
95   significant modulation of MMP and a decrease in mitochondrial energy production (ATP yield)
96   (Vanlerberghe, 2013). On the other hand, the channeling of electrons into AOX prevents ROS
97   overproduction under stress conditions (Vanlerberghe, Cvetkovska & Wang, 2009), thus,
98   electron distribution between the cytochrome *c* pathway and the AOX pathway can be regarded
99   as one of the most important factors in plant response to environmental pollutants, including
100 NSAIDs. Literature reports suggest that DCF in concentrations up to 12 mM in lupin (*Lupinus*
101 *polyphyllus*), pea (*Pisum sativum*), and lentil (*Lens culinaris*) increased activity of cytochrome *c*
102 oxidase in the cytosol, and decreased activity of this enzyme in seedling root mitochondria
103 (Ziółkowska et al., 2014). The exact reason for these changes is not clear. There is no literature
104 data concerning AOX functioning under DCF treatment, despite an increase in this enzyme's
105 activity having been observed in plants' response to other stresses, such as high temperature,
106 infection, or nutrient imbalance (Simons et al., 1999; Escobar, Geisler & Rasmusson, 2006;
107 Zalutskaya, Lapina & Ermilova, 2015). Therefore, it was decided to examine both cytochrome *c*
108 and AOX-pathway functioning in DCF-treated cells of the green alga *Chlamydomonas*
109 *reinhardtii*. The scheme of potential influence ways of DCF treatment on electron transport chain
110 in *Chlamydomonas reinhardtii* cells has been illustrated in Figure 1.
111   One of our earlier research projects showed that DCF affects cell cycle progression,
112 delaying cell division as compared to non-treated cells (Harshkova et al., 2021a). Since the cell
113 cycle progression seems to be tightly connected to changes in mitochondrial activity, number,
114 shape, size, and cellular location (Kianian & Kianian, 2014), and the differences in respiration
115 activity between young and mature cells may affect the sensitivity of cells to stress factors, it was
116 decided to use synchronous *C. reinhardtii* cultures (Pokora et al., 2017, 2018; Majewska et al.,
117 2018; Čížková et al., 2019) to eliminate the influence of the cell developmental stage on the
118 results. Based on our and other researchers' experience (Aksmann et al., 2014; Cross & Umen,
119 2015; Pokora et al., 2017; Čížková et al., 2019; Majewska et al., 2021; Harshkova et al.,

120   2021b,a), it was assumed that time points 0h, 3h, 6h, and 9h after the start of the light period of
121   the cell cycle coincides with the following stages: zoospores, young cells, adult cells, and mother
122   cells. Thus, oxygen consumption rate by the cells and mitochondrial activity parameters (MMP,
123   mtROS) were analyzed at those time points. Additionally, for illustration of MMP change,
124   confocal microscopy was used. Observation of the cell's structure organization by electron
125   microscope was included in analyses to check for any malformation in mitochondrial structures
126   during DCF exposure.

127

128   **Materials & Methods**

129

130   **Culture conditions and exposure to diclofenac**
131   Wild-type *Chlamydomonas reinhardtii* strain CC-1690 (Chlamydomonas Resource
132   Center, University of Minnesota, USA; https://www.chlamycollection.org/) was grown in 200-
133   mL glass vessels, in liquid HSM (High Salt Medium; pH 6.9 ± 0.1) (Harris, 2008), at 30°C.
134   Cultures were aerated with sterilized air (PTFE filter, Sartorius 2000) enriched with 2.5% (v/v)
135   CO_2 (Harshkova et al., 2021b). Photosynthetically active radiation intensity measured inside the
136   culture vessels was 250 ± 5 µmol photons $m^{-2} \cdot s^{-1}$, provided by white fluorescent tubes (OSRAM
137   Dulux L, 55W040) (Harshkova et al., 2021b). Population growth was synchronized by
138   alternating light and dark periods (L/D 10/14h); before the beginning of each light period, the
139   algal culture was diluted to a constant density of ca. 1.5×10^6 cells·mL^{-1} (Pokora et al., 2018). The
140   cultures were observed with a light microscope (Leica DM 1000 LED, Germany; magnification
141   10x40) to monitor synchronization. The synchronized population of daughter cells was used as
142   an inoculum for experimental cultures. At the beginning of each experiment, the algae were
143   treated with diclofenac (DCF) (diclofenac sodium salt, sodium;2-[2-(2,6-
144   dichloroanilino)phenyl]acetate; 98% purity, ABRC, Germany) dissolved in ddH$_2$O and added to
145   the culture to a final concentration of 135.5 mg·L^{-1}, corresponding to the toxicological value
146   EC50/24 (Majewska et al., 2018). The untreated population was set as a control. Cells were
147   sampled at 0h, 3h, 6h, or 9h after the start of the light period of the cell cycle, which
148   corresponded to the following phases of cell development: zoospores, young cells, adult cells,
149   and mother cells, respectively (Cross & Umen, 2015).
150   For examination by electron and confocal microscope, the algae cells were cultured as
151   described above, except for light/dark synchronization (Harris, 2008). Cultures with an initial
152   cell density of ca. 1.5×10^6 cells·mL^{-1} were divided into two sub-cultures: control or incubated
153   with DCF in a final concentration of 135.5 mg·L^{-1}. The cells were sampled after 24h incubation
154   and prepared for electron and confocal microscopy as described below (see subchapters below).

155

156   **Population density and cell volume**
157   The number and volume of cells were estimated using an electronic particle counter
158   (Beckman Coulter Z2) run by dedicated software.

159

160 **Cell's oxygen consumption rate**
161   Oxygen consumption rate was determined with a Clark-type oxygen electrode
162 (Oxygraph, Hansatech Ltd.). Before measurement, the cultures were darkened for 30 minutes to
163 stop photosynthesis, and all further steps were performed under dim light or in darkness. One mL
164 of cell suspension (about 1.5×10^6 cells·mL^{-1}) was sampled directly from the culture vessel and
165 placed in a measuring chamber of the Oxygraph. The cell suspension was stirred continuously,
166 and oxygen consumption measurements were carried out at 30°C in total darkness. The oxygen
167 consumption rate was expressed in nmol O_2 and recalculated per 1 million cells (nmol $O_2 \times 10^6$
168 cell^{-1}·min^{-1}). The data were obtained from three independent experiments with at least 2
169 biological replicates of each type of sample.
170
171 **Mitochondrial membrane potential (MMP) and mitochondrial ROS (mtROS) assessment**
172   Measurement of mitochondrial membrane potential (MMP) *in vivo* was performed by JC-
173 1-staining (5,5′,6,6′-Tetrachloro-1,1′,3,3′-tetraethyl-imidacarbocyanine iodide, Sigma-Aldrich)
174 based on protocol by Harshkova, Zielińska & Aksmann (2019). The stock solution of the
175 fluorochrome was prepared in DMSO (dimethyl sulfoxide, BioShop Canada). The final JC-1
176 concentration in the incubation mixture was 3 μM. The final concentration of DMSO in the
177 incubation mixture did not exceed 0.1% (v/v). At 0h, 3h, 6h, and 9h after the start of the light
178 period of the cell cycle, samples of the cell suspension were collected. Before the sampling, the
179 culture vessels were darkened for 30 min to stop photosynthetic processes. MMP was assessed
180 according to Harshkova, Zielińska & Aksmann (2019), with modification: cells were pelleted by
181 centrifugation for 5 min at 460 g in black test tubes and resuspended in HSM (heated to 30°C) to
182 obtain 1×10^6 cells·mL^{-1} for JC-1-staining. Measurement of MMP was performed after incubation
183 for 20 min in black 98-well plates, using the spectrofluorometer Varioskan Flash Microplate
184 Reader (Thermo Fisher Scientific, USA). The excitation wavelength for JC-1 was 488 nm, and
185 emission wavelengths were 538 and 596 nm (for monomers and oligomers of fluorochrome,
186 respectively). The data were obtained from two independent experiments with 2 biological
187 replications and with 2 technical replications of each sample measurement.
188   For confocal microscopy examination, the cell suspensions were centrifuged, and the
189 pellet (about 1×10^6 cells·mL^{-1}) was resuspended in a small volume of HSM and incubated with 3
190 μM JC-1. Stained with JC-1 cells were fixed with 4% paraformaldehyde in HEPES buffer for 1h
191 at RT (Craig & Avasthi, 2019). Cells were visualized with Leica STELLARIS 5 WLL confocal
192 microscopy with Ligtning module using FITC/TRITC ex/em. The photos presented are
193 maximum projections taken from z-stacks. with Lightning deconvolution combining signals
194 from the green-fluorescent JC-1 monomers (absorption/emission maxima ~514/529 nm) and the
195 red-fluorescent J-aggregates (emission maximum 590 nm). Mean fluorescence intensity of 10
196 representative cells of each experimental variant was quantified in triplicate using Leica
197 Application Suite X.
198   Mitochondrial ROS (mtROS) assessment was performed by MTO-staining
199 (MitoTracker™ Orange CM-H2TMRos, Thermo Fisher Scientific). Stock solutions of the

200 fluorochrome were prepared in DMSO. The final fluorochrome concentration in the incubation
201 mixture was 0.5 µM. The final concentration of DMSO in the incubation mixture did not exceed
202 0.1% (v/v). At 0h, 3h, 6h, and 9h after the start of the light period of the cell cycle, samples of
203 the cell suspension were collected. Before the sampling, the culture vessels were darkened for 30
204 min to stop photosynthetic processes. Cells were pelleted by centrifugation for 5 min at 460 g in
205 black test tubes and resuspended in HSM (heated to 30°C) to obtain 5×10^6 cells·mL^{-1}.
206 Measurement of mtROS was performed after incubation with MitoTracker™ Orange for 45 min
207 in black 98-well plates, using the spectrofluorometer Varioskan Flash Microplate Reader
208 (Thermo Fisher Scientific, USA). The excitation wavelength for MTO was 551 nm, and the
209 emission wavelength was 576 nm. The data were obtained from two independent experiments
210 with 2 biological replications and with 3 technical replications of each sample measurement.
211   To inhibit cytochrome *c* oxidase activity, potassium cyanide (KCN; Avantor Performance
212 Materials Poland), dissolved in ddH$_2$O was used. To inhibit alternative oxidase (AOX) activity,
213 salicylhydroxamic acid (SHAM; N,2-dihydroxybenzamide, Sigma-Aldrich) dissolved in DMSO
214 was prepared. Cell suspensions (15 mL) taken from the culture vessel were placed in a black
215 Falcon tube and incubated with 0.5 mM KCN (Ghosh et al., 2016) or with 3 mM SHAM (Liu et
216 al., 2021) for 5 min at 30°C. After the incubation, oxygen consumption rate, MMP and mtROS
217 were measured as described above.
218
219 **Ultrastructure examination**
220   For electron microscope examination, cell suspensions were centrifuged, and the pellet
221 (about $8\text{-}10 \times 10^6$ cells·mL^{-1}) was fixed overnight with 2.5% glutaraldehyde (Polysciences) in 0.1
222 M sodium cacodylate buffer, pH 7.2, then post-fixed with 2% osmium tetroxide (Agar) in 0.1 M
223 sodium cacodylate buffer. Further, cells were dehydrated with increasing concentrations of ethyl
224 alcohol, infiltrated, and embedded in Epon 812 resin (Sigma-Aldrich). Ultra-sections
225 (approximately 65 nm) were cut on Leica UC7. Sections were stained with uranyl acetate and
226 lead citrate and examined with a Tecnai Spirit BioTWIN transmission electron microscope
227 (FEI). The samples of cell suspensions were obtained from two independent experiments with at
228 least 2 biological replications.
229
230 **Statistical analysis**
231   Statistical analysis was performed using MS Excel 365 (Microsoft) and Statistica 13.3
232 (StatSoft). Statistica 13.3 (StatSoft) was used to compute a correlation matrix to measure the
233 strength of relationships between different variables and to compute the basic statistical and
234 nonparametric Mann-Whitney U-test when the population could not be assumed to be normally
235 distributed. A p-value < 0.05 was considered significant. A discriminant analysis was performed
236 to integrally evaluate the metabolic effects of diclofenac and compare them to ETC blockers.
237
238 **Results**
239

Population density and cell volume

The initial number of cells in the synchronic culture was set to $1.5 \times 10^6 \pm 0.44 \times 10^6$ cells$\cdot$mL^{-1}. The number of cells remained unchanged for 9h of the light period of the cell cycle in both the control and DCF-treated cultures (Tab. 1). The initial cell volume was 68.25 ± 8.06 fL, and in the control cultures reached about 540 ± 58.54 fL after 9h. In DCF-treated cultures the final cell volume was 23% lower than in the control (Tab. 1).

Cell's oxygen consumption rate

To estimate oxygen consumption rate, both control and DCF-treated cells were sampled at the 6th h of the cell cycle. In control cells, oxygen consumption rate was 21.91 ± 7.75 nmol $O_2 \times 10^6$ cell$^{-1}\cdot$min^{-1} (Fig. 2). The ETC-blockers, KCN and SHAM, caused a decrease in the oxygen consumption rate by 33-34% when applied separately and by 37% when applied in combination. In DCF-treated cells, the oxygen consumption rate reached about 150% of the control. Incubation of DCF-treated cells with KCN or SHAM caused a significant decrease in oxygen consumption rate, by 47% and 40%, respectively. The two blockers, when applied in combination, diminished oxygen consumption rate by 60% as compared to DCF-treated cells (Fig. 2).

Mitochondrial membrane potential (MMP) and mitochondrial ROS (mtROS) assessment

The value of MMP at the beginning of the experiment was 21.66 ± 2.52 a.u. After 3 hours of cell growth, the MMP did not differ between control and DCF-treated cells, but after 6 h and 9 h this parameter value was significantly lower in DCF-treated cells than in the control culture: 22.89 ± 11.54 a.u. in control cells and 10.33 ± 2.89 a.u. in DCF-treated cells after 6 h; 24.53 ± 7.96 a.u. in control cells and 8.17 ± 1.45 in DCF-treated cells after 9 h (Fig. 3, Tab. S1). MMP values were further diminished by SHAM and KCN + SHAM at 9th h of the experiment, to 13.52 ± 3.30 a.u. and 15.55 ± 1.19 a.u. in control cells, respectively (Fig. 3, Tab. S1).

To visualize the changes in membrane potential, cells treated with DCF for 24h were stained with JC-1 and examined using confocal microscopy (Fig. 4, Fig. S1). It was found that control cells exhibited strong red fluorescence ("C-red cells"), while in DCF-treated populations two fractions of cells could be seen, namely cells with a fluorescent signal similar to that of control cells ("DCF-red cells"), and cells exhibiting much weaker and more green fluorescence ("DCF-green cells") (Fig 4, Fig. S1). Measurements of fluorescence based on confocal microphotographs confirmed that "C-red cells" and "DCF-red cells" belong to the same statistical group while "DCF-green cells" significantly differ from them (results of fluorescence measurements are shown in Fig. S1).

The initial (0h) relative level of mtROS was 1.34 ± 0.33 a.u. At 3rd h of the cell cycle a statistically significant decrease of mtROS in DCF-treated cells (0.95 ± 0.26 a.u.) was noticed, as compared to control cells (1.52 ± 0.22 a.u.). A similar trend was observed in cells sampled at 6th h of the experiment (1.74 ± 0.47 a.u. for control and 0.88 ± 0.09 a.u. for DCF-treated cells,

279   respectively), and in cells sampled at 9th h of the cell cycle (1.13 ± 0.50 a.u. in control cells and

280   0.72 ± 0.15 a.u. in DCF-treated cells, respectively) (Tab. 2).

281

282   **Analysis of the cell's ultrastructure**

283   Analysis of the cell's ultrastructure revealed that pyrenoid (Py), clearly visible in the

284   control cells (Fig. 5A), was absent in DCF-treated cells, while the structure of thylakoids (th)

285   seemed to be unchanged (Fig. 5B). In the chloroplasts of DCF-treated cells, higher numbers of

286   large starch grains (s) could be seen (Fig. 5B). In DCF-treated cells vacuoles (v) were rare and

287   seemed to be converted into larger autophagic vacuoles (av) (Fig. 5B).

288   Examination of the mitochondria (m) structure in more detail led to the conclusion that in

289   the control cells, they were more regular, with correctly formed cristae (Fig. 6A). In DCF-treated

290   cells, mitochondria were larger, irregular, and swollen with few and degraded cristae but with

291   some inclusions or aggregates visible in the mitochondrial matrix (Fig. 6B).

292

293   **Discriminant analysis and correlation matrices of selected cell parameters**

294   Discriminant analysis and correlation matrices were created for three selected

295   physiological parameters, characterizing cells collected at 6th h of the cell cycle: MMP, oxygen

296   consumption rate, and cell volume. In the first step, the values of Wilks' lambda index were

297   calculated for all parameters to select the parameter with the most important discriminatory

298   contribution. The results indicated that MMP (Wilks' lambda = 0.3073) was the most influential.

299   The statistical significance of the value (p < 0.05) indicates good discrimination between all

300   experimental groups. Oxygen consumption made an additional discriminatory contribution

301   (partial lambda index, p < 0.05) in all cultures (Tab. 3).

302   Further, all areas were checked for the variable's standardization coefficients to enable

303   the construction of a reliable discriminant plot. MMP showed higher standardization coefficients

304   for variables (0.7998) in the area "root 1 *vs* root 2" compared to other areas (Tab. 4). Figure 7

305   demonstrates the discriminant plot in the area "root 1 *vs* root 2". It can be seen that the DCF-

306   treated cells were evenly separated from all other groups (Fig. 7).

307   To determine the cell responses to DCF more precisely compared to control cells, after

308   the discriminant analysis, each parameter was analyzed using correlation matrices (Spearman's

309   test) separately. Comparing the DCF action to the action of ETC-blockers on the control cells did

310   not reveal similarity (Tab. S2), except that for MMP Spearman's test showed a correlation (0.65,

311   p < 0.05) between the cells incubated with both KCN and SHAM vs. DCF-treated cells without

312   blockers (Tab. 5).

313

314   **Discussion**

315   The pollution of environment with NSAIDs is the emerging problem nowadays. The real

316   environmental concentrations of pharmaceuticals are reported to be in the range of nanograms

317   per liter, which is much lower than predicted environmental concentrations or predicted effective

318   concentrations (ECs) for aquatic organisms (Hejna et al. 2022). Also, DCF investigated in the

319 present work was shown to inhibit the growth of *Chlamydomonas reinhardtii* in a relatively high
320 concentration with EC50 = 135.5 mg/L (Majewska et al. 2018), while its concentrations noted in
321 water bodies reaches up to 10,200 ng/L (Hejna et al. 2022). However, because of continuous
322 input of DCF from wastewater and its bioaccumulation potential it can be assumed that chronic
323 effects of DCF to non-target organisms are stronger than acute effects. Moreover, drugs found in
324 the environment usually occur as mixtures, which are known to be much more toxic than the
325 individual substances (Cleuvers, 2003, 2004). Thus, analysis of DCF toxicity, using EC values
326 estimated in laboratory conditions, is an important component of ecotoxicological investigations.
327   Diclofenac has been reported as an inhibitor of population growth for microalgae species
328 such as *Chlamydomonas reinhardtii*, *Desmodesmus subspicatus*, and *Dunaliella tertiolecta*
329 (Cleuvers, 2003; Lin, Yu & Lin, 2008; Majewska et al., 2018). Some studies (Hájková et al.,
330 2019; Svobodníková et al., 2020) indicated that photosynthesis disruption and oxidative stress
331 induction in the cells were among the reasons for population growth inhibition by DCF. Similar
332 observations were described in our previous work (Majewska et al., 2018, 2021). Moreover, it
333 was reported (Harshkova et al., 2021b) that the treatment of *C. reinhardtii* with DCF in
334 concentration corresponding to the toxicological value EC50/24 can affect the growth of single
335 cell. Similar tendency was observed in the current work, namely the mature cells treated with
336 DCF were smaller than the control ones. Since the decrease in the cell size suggests disruption of
337 cellular energetics, analyses of mitochondria functioning seems to be good direction of the
338 investigations.
339   Interestingly, in the works by Majewska et al. (2018) and Harshkova et al. (2021b) no
340 respiration inhibition was found in DCF-treated cells of *Chlamydomonas reinhardtii* when
341 estimated based on oxygen consumption rate, despite such effects having been reported for other
342 organisms, including bacteria *Escherichia coli* (Liwarska-Bizukojc, Galamon & Bernat, 2018)
343 and animal cells, i.e., neuroblastoma cells (Darendelioglu, 2020) and cardiomyocytes (Ghosh et
344 al., 2016) during DCF-treatment. Unfortunately, there are few publications about dark respiration
345 and mitochondrial functioning in microalgal cells treated with NSAIDs. One of the reasons could
346 be difficulties in distinguishing between photosynthesis and respiration during investigations
347 because of tight cooperation between chloroplasts and mitochondria, and complexity of the
348 energetics and oxygen metabolism in photoautotrophic cells.
349   In the present work, not only oxygen consumption rate was analyzed, but also the
350 mitochondrial membrane potential was assessed using the fluorochrome JC-1, known for its
351 sensitivity in analyzing mitochondrial efficiency (Harshkova, Zielińska & Aksmann, 2019). For
352 revision of JC-1 staining suitability, the confocal microscope examination of *Chlamydomonas*
353 *reinhardtii* cells was used (Fig. 4). Additionally, mitochondrial ROS levels were measured using
354 the fluorochrome MitoTracker™ Orange CM-H2TMRos, a marker of mitochondrial oxidative
355 stress (Gonzalo et al., 2015; Martín-de-Lucía et al., 2018). Considering that parameters of
356 respiration efficiency (such as oxygen consumption rate, MMP, mitochondrial ultrastructure,
357 etc.) in algal cells, as well as their sensitivity to stress factors, are strongly influenced by cell

358 cycle phases (Ehara, Osafune & Hase, 1995), synchronous *C. reinhardtii* cultures were used for
359 these investigations.
360   Analysis of the results indicated that even short-time exposure of the cells to DCF
361 influences mitochondrial functioning. An increase in oxygen consumption rate suggested that
362 DCF stimulates dark respiration (Fig. 2). One of the possible explanations of this observation is
363 disruption of mitochondria-chloroplasts cooperation. This assumption is supported by the
364 literature data indicating that DCF negatively affects photosynthesis (Majewska et al. 2018,
365 2021) and that mitochondrial activity is particularly important for maintaining life processes in
366 cells with dysfunctional chloroplast (Araujo et al, 2014, Dang et al., 2014; Upadhyaya & Rao,
367 2019). In *C. reinhardtii* cells, mitochondria-chloroplasts interdependence, involving redox
368 control, energy balance, and organic compounds exchange, has been demonstrated in a wide
369 range of works. To mention only few examples, Dang et al. (2014) demonstrated that in *C.*
370 *reinhardtii* mutant *pgrl1*, deficient in PROTON GRADIENT REGULATION LIKE1 (PGRL1)
371 protein, acting as ferredoxin-quinone reductase, mitochondrial cooperation, and oxygen
372 photoreduction downstream of PSI is crucial for maintaining biomass productivity. Further, it
373 was shown that TOR kinase (target of rapamycin kinase) plays a key role in the regulation of
374 both chloroplast and mitochondria functions (Upadhyaya & Rao, 2019). TOR kinase inhibition
375 upon AZD-8055 treatment (selective TOR kinase inhibitor) leads to the dysregulation of
376 chloroplast and mitochondrial cooperation, increase in respiration rate and mitochondria
377 fragmentation, along with decrease in photosynthetic activity (Upadhyaya & Rao, 2019). On the
378 other hand, increased oxygen consumption rate observed in our work can result from
379 mitochondrial membrane damage and uncoupling effect, since increased oxygen uptake is
380 strictly connected with mitochondrial uncoupling (Baretto et al., 2020). Thus, to better explore
381 this problem and to try to separate the processes occurring in the mitochondria from those
382 occurring in the chloroplast, the MMP was analyzed.
383   It was found, that MMP tends to decrease after 3h of exposure to DCF (Fig. 3, Tab. S1)
384 and this decrease under DCF treatment is compatible with reports which emphasized the
385 reduction of MMP in cells treated with another common NSAID, indomethacin (Mazumder et
386 al., 2019). Visualization of JC-1-stained cells revealed, that in DCF-treated populations two
387 fractions of cells could be seen, namely cells with a fluorescent signal similar to that of control
388 cells, and cells exhibiting much weaker and more green fluorescence (Fig. S1). This suggests
389 that MMP decrease measured on population level (Fig. 3B) results from the appearance in the
390 population of a fraction of cells with severely disturbed metabolism rather than from an equal
391 reduction in the vital parameters of all cells in the population. It can be assumed that DCF
392 strongly affects cells that have already some developmental or metabolic dysfunctions. This
393 observation is consistent with the investigations reported by Majewska et al. (2018) that in DCF-
394 treated *C. reinhardtii* cells photosynthesis inhibition results mainly from "silencing" of some
395 fraction of the PS II reaction centers, while the reaction centers that remain active maintain their
396 normal operation. Also analyses of *C. reinhardtii* cell cycle under DCF-induced stress strongly
397 suggested, that some fraction of cells is eliminated from the population at the beginning of the

398   experiment, and in surviving cells physiological functions are affected only slightly (Harshkova

399   et al. 2021). Thus, the oxygen consumption rate and MMP measurements described above can be

400   interpreted on population, not on single cell level, which is important for ecotoxicological

401   investigations where population functioning is the main goal of research.

402   The above statement is valid also for another important observation made in the present

403   study, that the level of mtROS in DCF-treated populations was significantly lower than in

404   control ones (Tab. 2). These observations were surprising in light of the literature reports that

405   toxicity of many anthropogenic micropollutants, such as graphene oxide or poly(amidoamine)

406   dendrimers, towards *C. reinhardtii*, is related to an increase in mitochondrial ROS formation

407   accompanied by mitochondrial membrane depolarization and decreased mitochondrial activity

408   (Gonzalo et al., 2015; Martín-de-Lucía et al., 2018).

409   Searching for a possible explanation for these observations, it was decided to take a

410   closer look at the functioning of two ways of electron transport in the mitochondrial electron

411   transport chain, because *C. reinhardtii*, like other plants, has a standard cytochrome *c* pathway of

412   respiration as well as the alternative oxidase (AOX) pathway. The high activity of AOX results

413   in energy dissipation as heat and MMP decrease, which on the one hand causes a reduction of

414   ATP production (Millenaar & Lambers, 2003), but on the other hand plays an important role in

415   stress response (Zalutskaya, Lapina & Ermilova, 2015). It was shown that AOX genes are

416   upregulated under stress conditions such as H_2O_2, heat, high light illumination, nutrients

417   limitation, and that AOX knockdown results in hypersensitivity to stress, as it was described for

418   AOX-antisense lines of *Phaeodactylum tricornutum* (Murik et al., 2019). In the antisense line of

419   this diatom also photosynthesis was strongly affected, and AOX disfunction had a significant

420   effect on gene expression and metabolome profile. Further, it was shown (Mathy et al., 2010)

421   that *C. reinhardtii* cells with reduced levels of *AOX1* (one of the AOX genes) exhibited hyper-

422   reduction of the respiratory chain and elevated production of ROS relative to wild-type cells, as

423   well as an increase activity of enzymes involved in anabolic pathways and a decrease activity of

424   enzymes of the main catabolic pathways. Moreover, it was reported that in young cells the AOX-

425   dependent electron transport is relatively low, while at advanced stages of cell development,

426   AOX's relative contribution to oxygen consumption increases, so there may be differences in the

427   sensitivity of young and mature cells to external toxic factors (for example DCF) depending on

428   the leading respiratory pathways (Strenkert et al., 2019). Indeed, a comparison of the results of

429   MMP measurements obtained from treatment with respiratory blockers allows us to conclude

430   that mature cells are more sensitive to SHAM (AOX selective inhibitor) than the younger cells,

431   and that this effect is further enhanced by DCF (Fig. 3, Tab. S1). Because the response of

432   respiration efficiency parameters (oxygen consumption rate and MMP) to selective respiratory

433   blockers (KCN for cytochrome *c* oxidase and SHAM for AOX) and their response to DCF are

434   not comparable (Fig. 2 and Fig. 3, Tab. S1), it can be suggested that DCF impact on

435   mitochondrial respiration is non-specific. This suggestion is supported by the statistical analyses,

436   which did not reveal a similarity between cells' response to respiratory blockers applied

437   separately, and cells' response to DCF (Fig. 7 and Tab. 5). The tendency for increased oxygen

438   consumption rate (Fig. 2 in this study; (Harshkova et al., 2021b)) with low MMP and low
439   mtROS production in DCF-treated populations may indicate an uncoupling of oxidative
440   phosphorylation due to destruction of mitochondrial membranes. Destruction of mitochondrial
441   membranes accompanied by uncoupling of oxidative phosphorylation has been documented for
442   animal mitochondria treated with aspirin, indomethacin, naproxen, and piroxicam
443   (Somasundaram et al., 1997).
444   To verify the assumption about non-specific DCF impact, the ultrastructure of
445   *Chlamydomonas* cells was analyzed. To obtain a clear picture of the possible changes in the cell
446   structure, a relatively long period of DCF treatment (24h) was applied. The electron micrographs
447   confirmed malformation in mitochondrial structures of cells suffering from DCF-induced stress
448   (Fig. 5 and Fig. 6). The elongated mitochondria, irregular with degraded cristae forms, may
449   suggest mitochondrial hyper-fission as a subcellular effect of DCF, as was reported for
450   indomethacin-treated animal mitochondria (Mazumder et al., 2019). Ultrastructure analysis also
451   revealed other DCF-induced changes, namely the disappearance of the pyrenoid in the
452   chloroplast and the intensification of chloroplast starch deposition. The latter effect is consistent
453   with observation reported by Harshkova et al. (Harshkova et al., 2021a) that DCF causes a shift
454   in material and energy balance toward carbohydrate storage (starch) in *C. reinhardtii* cells. The
455   accumulation of starch in microalgal cultures under stress conditions also was reported by other
456   authors (Ivanov et al., 2021). Thus, the mitochondrial dysfunctions observed in the present work
457   may be one of the causes of previously reported cell developmental disorders and alterations in
458   the cell cycle (Harshkova et al., 2021a).
459

Conclusions

461   The results obtained in this work suggest that DCF strongly affects this fraction of cells,
462   that have some developmental or metabolic dysfunctions, while more vital cells are affected only
463   slightly, as it was already indicated in literature (see "Discussion"). In the cells suffering from
464   DCF treatment, the drug influence on mitochondria functioning in a non-specific way, destroying
465   the structure of mitochondrial membranes. This primary effect led to the uncoupling of oxidative
466   phosphorylation. Since in algal cells mitochondria are important sources of metabolites,
467   signaling molecules, and energy during both light and dark phases of the cell cycle, it can be
468   assumed that mitochondrial dysfunction is an important factor in DCF phytotoxicity and
469   impairment of cell development observed in other works (Harshkova et al., 2021a,b). Because
470   studies of the effects of NSAIDs on the functioning of plant mitochondria are relatively scarce,
471   the present work is an important contribution to the elucidation of the mechanism of NSAID
472   toxicity toward non-target plant organisms.
473

References

475   Van Aken O, Giraud E, Clifton R, Whelan J. 2009. Alternative oxidase: a target and regulator of
476   stress responses. *Physiologia Plantarum* 137:354–361. DOI: 10.1111/j.1399-
477   3054.2009.01240.x.
478   Aksmann A, Pokora W, Baścik-Remisiewicz A, Dettlaff-Pokora A, Wielgomas B, Dziadziuszko

479   M, Tukaj Z. 2014. Time-dependent changes in antioxidative enzyme expression and
480   photosynthetic activity of Chlamydomonas reinhardtii cells under acute exposure to
481   cadmium and anthracene. *Ecotoxicology and Environmental Safety* 110:31–40. DOI:
482   10.1016/j.ecoenv.2014.08.005.
483 Araújo, W. L., Nunes-Nesi, A., Fernie, A. R., 2014. On the role of plant mitochondrial
484   metabolism and its impact on photosynthesis in both optimal and sub-optimal growth
485   conditions. *Photosynthesis research* 119: 141-156. DOI: 10.1007/s11120-013-9807-4.
486 Barreto, P., Counago, R. M., Arruda, P., 2020. Mitochondrial uncoupling protein-dependent
487   signaling in plant bioenergetics and stress response. *Mitochondrion* 53: 109-120. DOI:
488   10.1016/j.mito.2020.05.001.
489 Čížková M, Slavková M, Vítová M, Zachleder V, Bišová K. 2019. Response of the Green Alga
490   Chlamydomonas reinhardtii to the DNA Damaging Agent Zeocin. *Cells* 8:735. DOI:
491   10.3390/cells8070735.
492 Cleuvers M. 2003. Aquatic ecotoxicity of pharmaceuticals including the assessment of
493   combination effects. *Toxicology Letters* 142:185–194. DOI: 10.1016/S0378-
494   4274(03)00068-7.
495 Cleuvers, M. 2004. Mixture toxicity of the anti-inflammatory drugs diclofenac, ibuprofen,
496   naproxen, and acetylsalicylic acid. *Ecotoxicology and Environmental Safety* 59: 309–315.
497   DOI: 10.1016/S0147-6513(03)00141-6.
498 Copolovici L, Timis D, Taschina M, Copolovici D, Cioca G, Bungau S. 2017. Diclofenac
499   Influence on Photosynthetic Parameters and Volatile Organic Compounds Emision from
500   Phaseolus vulgaris L.Plants. *Revista de Chimie* 68:2076–2078. DOI:
501   10.37358/RC.17.9.5826.
502 Craig EW, Avasthi P. 2019. Visualizing Filamentous Actin Using Phalloidin in Chlamydomonas
503   reinhardtii. *Bio-protocol* 9(12):e3274. DOI: 10.21769/BioProtoc.3274.Cross FR, Umen JG.
504   2015. The Chlamydomonas cell cycle. *The Plant Journal* 82:370–392. DOI:
505   10.1111/tpj.12795.
506 Dang KV, Plet J, Tolleter D, Jokel M, Cuiné S, Carrier P, Auroy P, Richaud P, Johnson X, Alric
507   J, Allahverdiyeva Y, Peltier G., 2014. Combined increases in mitochondrial cooperation and
508   oxygen photoreduction compensate for deficiency in cyclic electron flow in
509   Chlamydomonas reinhardtii. *Plant Cell*. 26(7): 3036-50. DOI: 10.1105/tpc.114.126375
510 Darendelioglu E. 2020. Neuroprotective Effects of Chrysin on Diclofenac-Induced Apoptosis in
511   SH-SY5Y Cells. *Neurochemical Research*:1–8. DOI: 10.1007/s11064-020-02982-8.
512 Ehara T, Osafune T, Hase E. 1995. Behavior of mitochondria in synchronized cells of
513   Chlamydomonas reinhardtii (Chlorophyta). *Journal of Cell Science* 108:499–507. DOI:
514   10.1242/jcs.108.2.499.
515 Escobar MA, Geisler DA, Rasmusson AG. 2006. Reorganization of the alternative pathways of
516   the Arabidopsis respiratory chain by nitrogen supply: opposing effects of ammonium and
517   nitrate. *The Plant Journal* 45:775–788. DOI: 10.1111/j.1365-313X.2005.02640.x.
518 Ghosh R, Goswami SK, Feitoza LFBB, Hammock B, Gomes A V. 2016. Diclofenac induces
519   proteasome and mitochondrial dysfunction in murine cardiomyocytes and hearts.
520   *International Journal of Cardiology* 223:923–935. DOI: 10.1016/j.ijcard.2016.08.233.
521 Gonzalo S, Rodea-Palomares I, Leganés F, García-Calvo E, Rosal R, Fernández-Piñas F. 2015.
522   First evidences of PAMAM dendrimer internalization in microorganisms of environmental
523   relevance: A linkage with toxicity and oxidative stress. *Nanotoxicology* 9:706–718. DOI:
524   10.3109/17435390.2014.969345.

525 Hájková M, Kummerová M, Zezulka Š, Babula P, Váczi P. 2019. Diclofenac as an
526   environmental threat: Impact on the photosynthetic processes of Lemna minor chloroplasts.
527   *Chemosphere* 224:892–899. DOI: 10.1016/j.chemosphere.2019.02.197.

528 Harris EH. 2008. *The Chlamydomonas Sourcebook : Introduction to Chlamydomonas and Its*
529   *Laboratory Use.* Elsevier.

530 Harshkova D, Liakh I, Bialevich V, Ondrejmišková K, Aksmann A, Bišová K. 2021a.
531   Diclofenac Alters the Cell Cycle Progression of the Green Alga Chlamydomonas
532   reinhardtii. *Cells* 10:1936. DOI: 10.3390/cells10081936.

533 Harshkova D, Majewska M, Pokora W, Baścik-Remisiewicz A, Tułodziecki S, Aksmann A.
534   2021b. Diclofenac and atrazine restrict the growth of a synchronous Chlamydomonas
535   reinhardtii population via various mechanisms. *Aquatic Toxicology* 230:105698. DOI:
536   10.1016/j.aquatox.2020.105698.

537 Harshkova D, Zielińska E, Aksmann A. 2019. Optimization of a microplate reader method for
538   the analysis of changes in mitochondrial membrane potential in Chlamydomonas reinhardtii
539   cells using the fluorochrome JC-1. *Journal of Applied Phycology* 31:3691–3697. DOI:
540   10.1007/s10811-019-01860-3.

541 He B shu, Wang J, Liu J, Hu X min. 2017. Eco-pharmacovigilance of non-steroidal anti-
542   inflammatory drugs: Necessity and opportunities. *Chemosphere* 181:178–189. DOI:
543   10.1016/j.chemosphere.2017.04.084.

544 Hejna M, Kapuścińska D, Aksmann A. 2022. Pharmaceuticals in the Aquatic Environment: A
545   Review on Eco-Toxicology and the Remediation Potential of Algae. *International Journal*
546   *of Environmental Research and Public Health* 19:7717. DOI: 10.3390/ijerph19137717.

547 Ivanov IN, Zachleder V, Vítová M, Barbosa MJ, Bišová K. 2021. Starch Production in
548   Chlamydomonas reinhardtii through Supraoptimal Temperature in a Pilot-Scale
549   Photobioreactor. *Cells* 10:1084. DOI: 10.3390/cells10051084.

550 Kianian PMA, Kianian SF. 2014. Mitochondrial dynamics and the cell cycle. *Frontiers in Plant*
551   *Science* 5:1–7. DOI: 10.3389/fpls.2014.00222.

552 Kummerová M, Zezulka Š, Babula P, Tříska J. 2016. Possible ecological risk of two
553   pharmaceuticals diclofenac and paracetamol demonstrated on a model plant Lemna minor.
554   *Journal of Hazardous Materials* 302:351–361. DOI: 10.1016/j.jhazmat.2015.09.057.

555 Lin AY-C, Yu T-H, Lin C-F. 2008. Pharmaceutical contamination in residential, industrial, and
556   agricultural waste streams: Risk to aqueous environments in Taiwan. *Chemosphere* 74:131–
557   141. DOI: 10.1016/j.chemosphere.2008.08.027.

558 Liu Y, Yu L-L, Peng Y, Geng X-X, Xu F. 2021. Alternative Oxidase Inhibition Impairs Tobacco
559   Root Development and Root Hair Formation. *Frontiers in Plant Science* 12. DOI:
560   10.3389/fpls.2021.664792.

561 Liwarska-Bizukojc E, Galamon M, Bernat P. 2018. Kinetics of Biological Removal of the
562   Selected Micropollutants and Their Effect on Activated Sludge Biomass. *Water, Air, & Soil*
563   *Pollution* 229:356. DOI: 10.1007/s11270-018-4015-7.

564 Majewska M, Harshkova D, Guściora M, Aksmann A. 2018. Phytotoxic activity of diclofenac:
565   Evaluation using a model green alga Chlamydomonas reinhardtii with atrazine as a
566   reference substance. *Chemosphere* 209:989–997. DOI:
567   10.1016/j.chemosphere.2018.06.156.

568 Majewska M, Harshkova D, Pokora W, Baścik-Remisiewicz A, Tułodziecki S, Aksmann A.
569   2021. Does diclofenac act like a photosynthetic herbicide on green algae? Chlamydomonas
570   reinhardtii synchronous culture-based study with atrazine as reference. *Ecotoxicology and*

571   *Environmental Safety* 208:111630. DOI: 10.1016/j.ecoenv.2020.111630.
572   Martín-de-Lucía I, Campos-Mañas MC, Agüera A, Leganés F, Fernández-Piñas F, Rosal R.
573   2018. Combined toxicity of graphene oxide and wastewater to the green alga
574   Chlamydomonas reinhardtii. *Environmental Science: Nano* 5:1729–1744. DOI:
575   10.1039/C8EN00138C.
576   Mathy G, Cardol P, Dinant M, Blomme A, Gérin S, Cloes M, Ghysels B, DePauw E, Leprince P,
577   Remacle C, Sluse-Goffart C, Franck F, Matagne RF, Sluse FE. 2010. Proteomic and
578   Functional Characterization of a Chlamydomonas reinhardtii Mutant Lacking the
579   Mitochondrial Alternative Oxidase 1. *Journal of Proteome Research* 9:2825–2838. DOI:
580   10.1021/pr900866e.
581   Mazumder S, De R, Debsharma S, Bindu S, Maity P, Sarkar S, Saha SJ, Siddiqui AA, Banerjee
582   C, Nag S, Saha D, Pramanik S, Mitra K, Bandyopadhyay U. 2019. Indomethacin impairs
583   mitochondrial dynamics by activating the PKCζ–p38–DRP1 pathway and inducing
584   apoptosis in gastric cancer and normal mucosal cells. *Journal of Biological Chemistry*
585   294:8238–8258. DOI: 10.1074/jbc.RA118.004415.
586   Millenaar FF, Lambers H. 2003. The Alternative Oxidase: in vivo Regulation and Function.
587   *Plant Biology* 5:2–15. DOI: 10.1055/s-2003-37974.
588   Møller IM, Rasmusson AG, Van Aken O. 2021. Plant mitochondria - past, present and future.
589   *The Plant journal : for cell and molecular biology* 108:912–959. DOI: 10.1111/tpj.15495.
590   Mulkiewicz E, Wolecki D, Świacka K, Kumirska J, Stepnowski P, Caban M. 2021. Metabolism
591   of non-steroidal anti-inflammatory drugs by non-target wild-living organisms. *Science of*
592   *The Total Environment* 791:148251. DOI: 10.1016/j.scitotenv.2021.148251.
593   Murik O, Tirichine L, Prihoda J, Thomas Y, Araújo WL, Allen AE, Fernie AR, Bowler C., 2019.
594   Downregulation of mitochondrial alternative oxidase affects chloroplast function, redox
595   status and stress response in a marine diatom. *New Phytologist* 221(3):1303-1316. DOI:
596   10.1111/nph.15479.Ortúzar M, Esterhuizen M, Olicón-Hernández DR, González-López J,
597   Aranda E. 2022. Pharmaceutical Pollution in Aquatic Environments: A Concise Review of
598   Environmental Impacts and Bioremediation Systems. *Frontiers in Microbiology* 13. DOI:
599   10.3389/fmicb.2022.869332.
600   Ben Ouada S, Ben Ali R, Cimetiere N, Leboulanger C, Ben Ouada H, Sayadi S. 2019.
601   Biodegradation of diclofenac by two green microalgae: Picocystis sp. and Graesiella sp.
602   *Ecotoxicology and Environmental Safety* 186:109769. DOI: 10.1016/j.ecoenv.2019.109769.
603   Pokora W, Aksmann A, Baścik-Remisiewicz A, Dettlaff-Pokora A, Rykaczewski M, Gappa M,
604   Tukaj Z. 2017. Changes in nitric oxide/hydrogen peroxide content and cell cycle
605   progression: Study with synchronized cultures of green alga Chlamydomonas reinhardtii.
606   *Journal of Plant Physiology* 208:84–93. DOI: 10.1016/j.jplph.2016.10.008.
607   Pokora W, Aksmann A, Baścik-Remisiewicz A, Dettlaff-Pokora A, Tukaj Z. 2018. Exogenously
608   applied hydrogen peroxide modifies the course of the Chlamydomonas reinhardtii cell
609   cycle. *Journal of Plant Physiology* 230:61–72. DOI: 10.1016/j.jplph.2018.07.015.
610   Schmidt W, Redshaw CH. 2015. Evaluation of biological endpoints in crop plants after exposure
611   to non-steroidal anti-inflammatory drugs (NSAIDs): Implications for phytotoxicological
612   assessment of novel contaminants. *Ecotoxicology and Environmental Safety* 112:212–222.
613   DOI: 10.1016/j.ecoenv.2014.11.008.
614   Simons BH, Millenaar FF, Mulder L, Van Loon LC, Lambers H. 1999. Enhanced Expression
615   and Activation of the Alternative Oxidase during Infection of Arabidopsis with
616   Pseudomonas syringae pv tomato1. *Plant Physiology* 120:529–538. DOI:

617   10.1104/pp.120.2.529.
618   Somasundaram S, Rafi S, Hayllar J, Sigthorsson G, Jacob M, Price AB, Macpherson A, Mahmod
619   T, Scott D, Wrigglesworth JM, Bjarnason I. 1997. Mitochondrial damage: a possible
620   mechanism of the "topical" phase of NSAID induced injury to the rat intestine. *Gut* 41:344–
621   353. DOI: 10.1136/gut.41.3.344.
622   Strenkert D, Schmollinger S, Gallaher SD, Salomé PA, Purvine SO, Nicora CD, Mettler-
623   Altmann T, Soubeyrand E, Weber APM, Lipton MS, Basset GJ, Merchant SS. 2019.
624   Multiomics resolution of molecular events during a day in the life of Chlamydomonas.
625   *Proceedings of the National Academy of Sciences* 116:2374–2383. DOI:
626   10.1073/pnas.1815238116.
627   Svobodníková L, Kummerová M, Zezulka Š, Babula P, Sendecká K. 2020. Root response in
628   Pisum sativum under naproxen stress: Morpho-anatomical, cytological, and biochemical
629   traits. *Chemosphere* 258. DOI: 10.1016/j.chemosphere.2020.127411.
630   Upadhyaya S, Rao BJ. 2019. Reciprocal regulation of photosynthesis and mitochondrial
631   respiration by TOR kinase in Chlamydomonas reinhardtii. *Plant Direct* 3(11): e00184. DOI:
632   10.1002/pld3.184.
633   Vanlerberghe GC. 2013. Alternative Oxidase: A Mitochondrial Respiratory Pathway to Maintain
634   Metabolic and Signaling Homeostasis during Abiotic and Biotic Stress in Plants.
635   *International Journal of Molecular Sciences* 14:6805–6847. DOI: 10.3390/ijms14046805.
636   Vanlerberghe GC, Cvetkovska M, Wang J. 2009. Is the maintenance of homeostatic
637   mitochondrial signaling during stress a physiological role for alternative oxidase?
638   *Physiologia Plantarum* 137:392–406. DOI: 10.1111/j.1399-3054.2009.01254.x.
639   Zalutskaya Z, Lapina T, Ermilova E. 2015. The Chlamydomonas reinhardtii alternative oxidase 1
640   is regulated by heat stress. *Plant Physiology and Biochemistry* 97:229–234. DOI:
641   10.1016/j.plaphy.2015.10.014.
642   Ziółkowska A, Piotrowicz-Cieślak AI, Rydzyński D, Adomas B, Nałecz-Jawecki G. 2014.
643   Biomarkers of leguminous plant viability in response to soil contamination with diclofenac.
644   *Polish Journal of Environmental Studies* 23:263–269.
645   Zorova LD, Popkov VA, Plotnikov EY, Silachev DN, Pevzner IB, Jankauskas SS, Babenko VA,
646   Zorov SD, Balakireva A V., Juhaszova M, Sollott SJ, Zorov DB. 2018. Mitochondrial
647   membrane potential. *Analytical Biochemistry* 552:50–59. DOI: 10.1016/j.ab.2017.07.009.
648

The cell volume and population density in control and DCF-treated *Chlamydomonas reinhardtii* cultures.

DCF was applied to the culture at 0h at a concentration of 135.5 mg•L^{-1}. Data are presented as mean ± SD. * indicates statistically significant differences between control and treated populations ($p < 0.05$; Mann–Whitney U test; $n = 8$).

	0h	3h	6h	9h
Cell volume (fL)				
control	68.25 ± 8.06	149.90 ± 17.96	307.39 ± 45.66	539.61 ± 58.54
DCF	68.25 ± 8.06	135.15 ± 21.89	**$217.26 \pm 63.29*$**	**$414.85 \pm 31.35*$**
Population density ($\times 10^6$ cells mL^{-1})				
control	1.54 ± 0.04	1.66 ± 0.14	1.80 ± 0.18	2.04 ± 0.25
DCF	1.54 ± 0.04	1.69 ± 0.10	1.77 ± 0.28	1.76 ± 0.24

Relative level of mtROS in *Chlamydomonas reinhardtii* cells.

DCF was applied to the culture at 0h of the experiment at a concentration of 135.5 mg•L^{-1}. Data shown as % of control were originally expressed in a.u. of mtROS ± SD. * indicates statistically significant differences between control and treated populations ($p < 0.05$; Mann–Whitney U test; n = 12).

	0h	3h	6h	9h
control	100.0±24.3	100.0±14.2	100.0±27.0	100.0±43.9
DCF	100.0±24.3	**62.5±27.3 ***	**50.6±9.9 ***	**64.0±20.3 ***

Discriminant analysis of MMP, oxygen consumption rate, and cell volume in *Chlamydomonas reinhardtii* control cells and DCF-treated cells, incubated with ETC-blockers or non-blocked.

The cells were sampled at 6th h of the cell cycle. * indicates statistically significant differences between cultures at $p < 0.05$ (Mann–Whitney U test; n = 8).

	Wilks' lambda	partial lambda	F-remove (4.23)	p
MMP, a.u.	**0.3073***	**0.32582***	**11.8997***	$p < 0.05$
oxygen consumption rate, nmol $O_2 \times 10^6$ cells^{-1}·min^{-1}	**0.1696***	**0.5904***	**3.9892***	$p < 0.05$
cell volume, fL	0.1440	0.6954	2.5190	0.0690

Standardization coefficients for canonical variables in the discriminant analysis of MMP, oxygen consumption rates, and cell volume in *Chlamydomonas reinhardtii* control cells and DCF-treated cells, incubated with ETC-blockers or non-blocked.

Cells were sampled at 6th h of the cell cycle, n = 8.

	Root 1	Root 2	Root 3
MMP, a.u.	0.7998	-0.6402	-0.0574
oxygen consumption rates, nmol $O_2 \times 10^6$ cells $^{-1}$·min $^{-1}$	-0.3580	-0.7610	0.5655
cell volume, fL	0.5245	0.3282	0.8017

Correlation matrices (Spearman's test) for values of MMP.

KCN = potassium cyanide-incubated cells; SHAM = salicylhydroxamic acid-incubated cells;
DCF = DCF-treated cells. * indicates statistically significant correlation between groups at p
< 0.05.

	KCN	SHAM	KCN + SHAM	DCF
KCN	1.0000	0.4196	0.1468	0.3636
SHAM	0.4196	1.0000	0.0909	-0.0559
KCN + SHAM	0.1468	0.0909	1.0000	**0.65035***
DCF	0.3636	-0.0559	**0.65035***	1.0000

Figure 1

The scheme of electron transport chain in algal mitochondria with the sites of KCN and SHAM action marked.

I, II, III, IV = mitochondrial complexes I (NADH-ubiquinone oxidoreductase), II (succinate dehydrogenase), III (ubiquinol–cytochrome *c* oxidoreductase), and IV (cytochrome *c* oxidase); AOX = alternative oxidase; Cyt *c* = cytochrome *c*.

[p]Created with BioRender.com (individual subscription). Adapted from "Electron Transport Chain", by BioRender.com (2024). Retrieved from https://app.biorender.com/biorender-templates.[p]
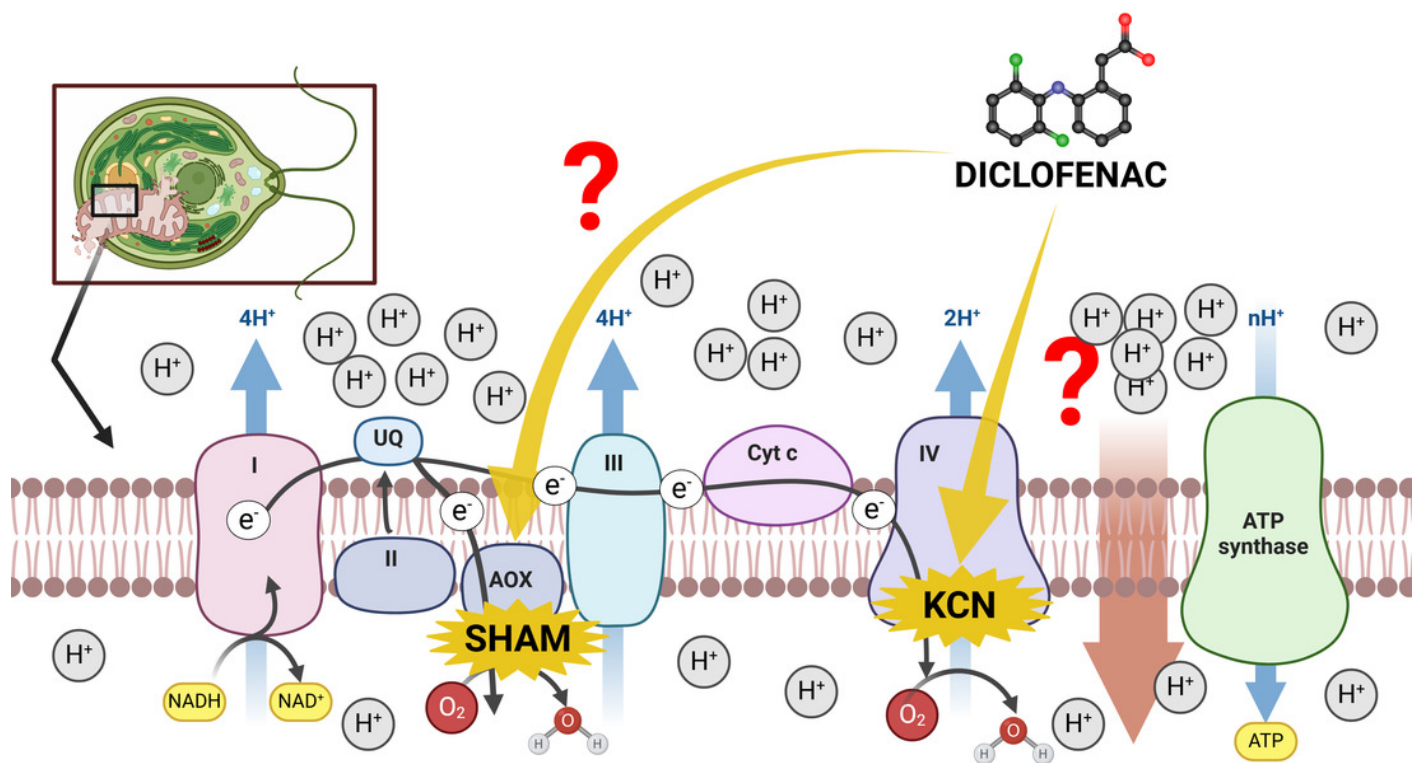
Figure 2

The influence of ETC-blockers on oxygen consumption rate in control and DCF-treated cells of *Chlamydomonas reinhardtii* at 6th h of the light phase of the cell cycle.

DCF was applied to the culture at the beginning of the cell cycle (0h) at a concentration of 135.5 mg•L^{-1}. KCN = potassium cyanide-incubated cells; SHAM = salicylhydroxamic acid–incubated cells; DCF = cells treated with diclofenac. Data are given in nmol $O_2 \times 10^6$ $cell^{-1}$•min^{-1} ± SD. * indicates statistically significant differences between control and treated populations, p <0.05 (Mann–Whitney U test; n = 8). ^{o} indicates statistically significant differences compared to the DCF-treated cells without blockers, p < 0.05 (Mann–Whitney U test; n = 8).
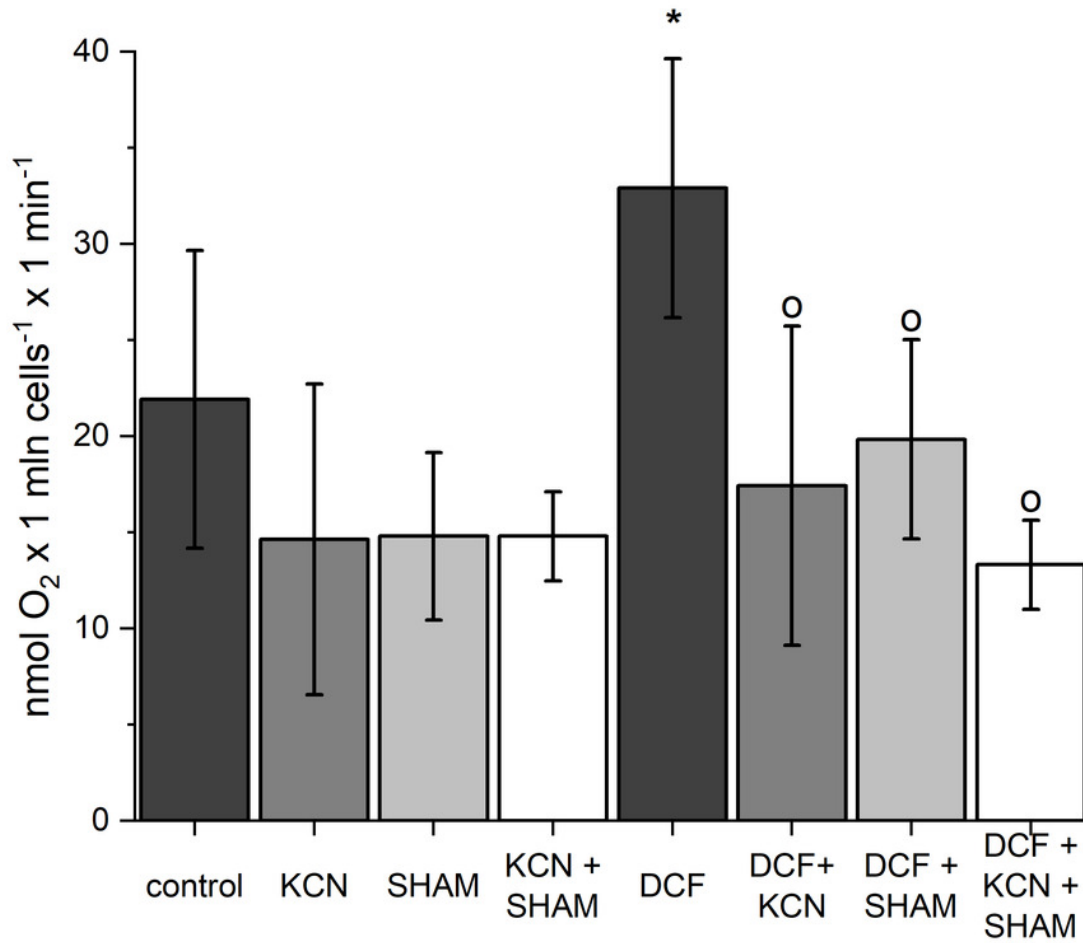
Figure 3

Mitochondrial membrane potential in control (A) and DCF-treated (B) *Chlamydomonas reinhardtii* cells.

DCF was applied to the culture at the beginning of the cell cycle (0h) at a concentration of 135.5 mg•L^{-1}. KCN = potassium cyanide-incubated cells; SHAM = salicylhydroxamic acid–incubated cells; DCF = cells treated with diclofenac. Data are given in a.u of MMP ± SD. * indicates statistically significant differences between control and treated populations, p < 0.05 (Mann–Whitney U test; n = 8).
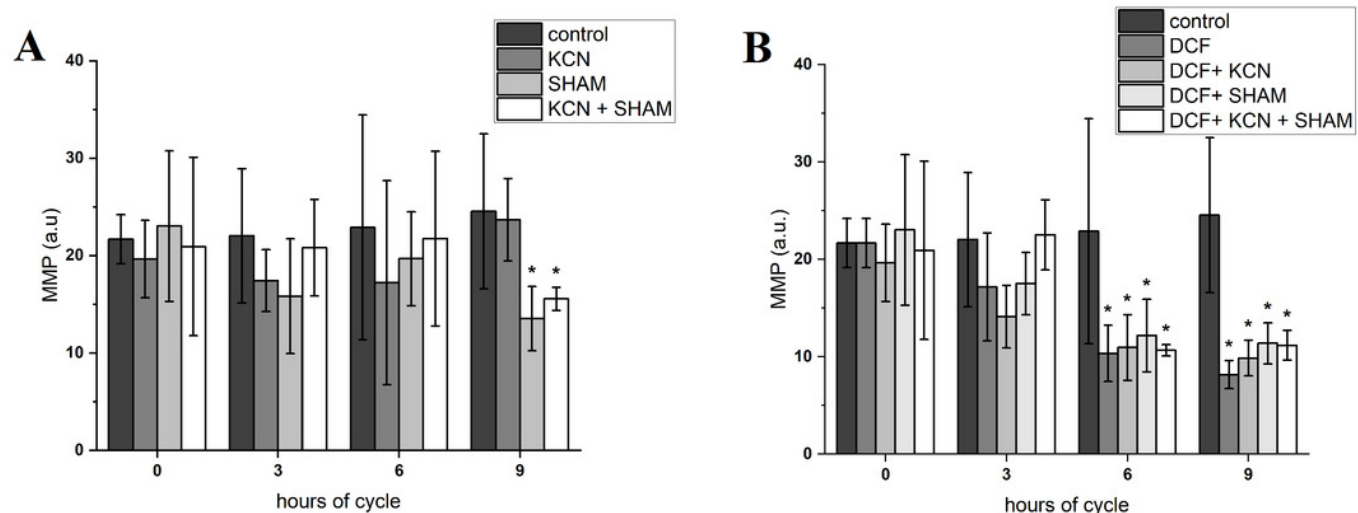
Figure 4

Visualization of JC-1 fluorescence in *Chlamydomonas reinhardtii* cells, control (A) and treated with DCF (B).

DCF was applied to the culture at 0h of the experiment at a concentration of 135.5 mg•L^{-1}. (A) Control population with cells exhibiting strong red-fluorescent J-aggregates ("C-red cells"; max. emission ~590 nm). (B) Cells treated with DCF for 24h, with two different cell populations: "DCF-red cells", i.e., cells with strong red fluorescence of J-aggregates, and "DCF-green cells" i.e., cells with much weaker and mainly green fluorescence of J-monomers (max. emission ~529 nm).
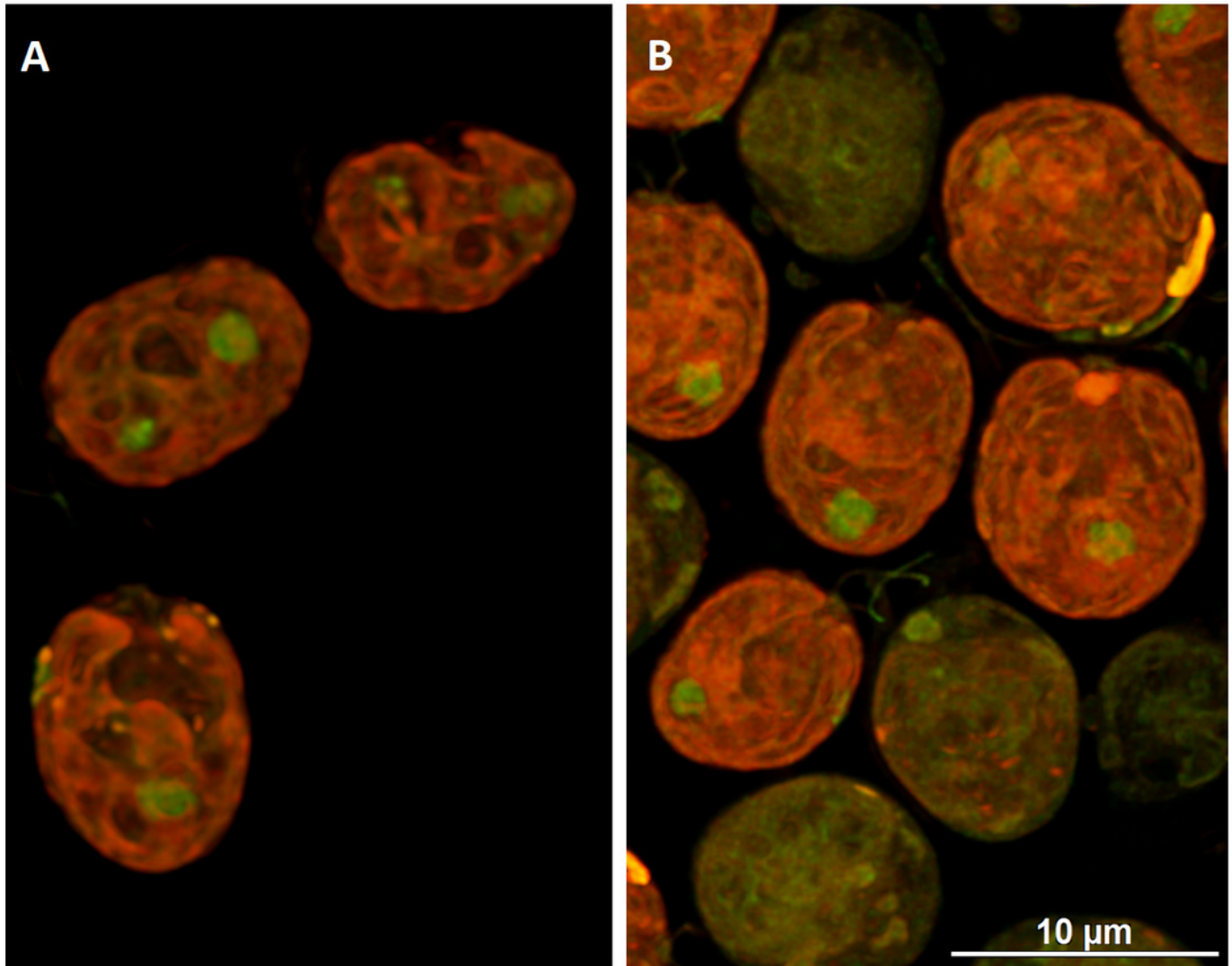
Figure 5

Electron microphotographs of cell structures in control (A) and DCF-treated (B) *Chlamydomonas reinhardtii* cells.

DCF was applied to the culture at the beginning of the experiment (0h) at a concentration of 135.5 mg·L^{-1} and cells were sampled after 24h. Bar = 1 μm. N - nucleus, Ch - chloroplast, s - starch grain, Py - pyrenoid, m - mitochondria, v - vacuole, av - autophagic vacuole, black arrow - eyespot.
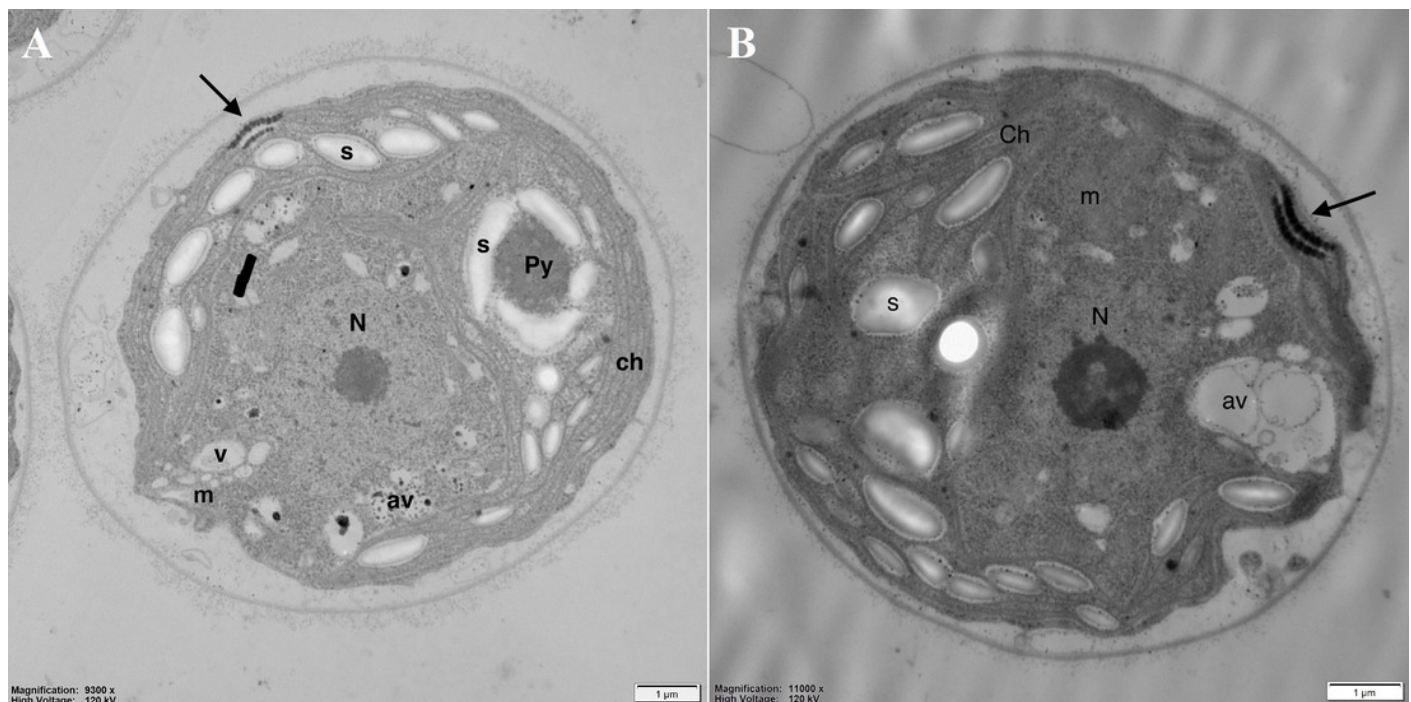
Figure 6

Electron microphotographs of mitochondria structures in control (A) and DCF-treated (B) *Chlamydomonas reinhardtii* cells.

DCF was applied to the culture at the beginning of the cell cycle (0 h) at a concentration of 135.5 mg•L^{-1}, and cells were sampled after 24h. Bar = 200 nm. Ch - chloroplast, s - starch grain, th - thylakoid, m - mitochondria, cw - cell wall, v - vacuole. Irregular structures of mitochondria with degraded cristae are marked as white arrows.
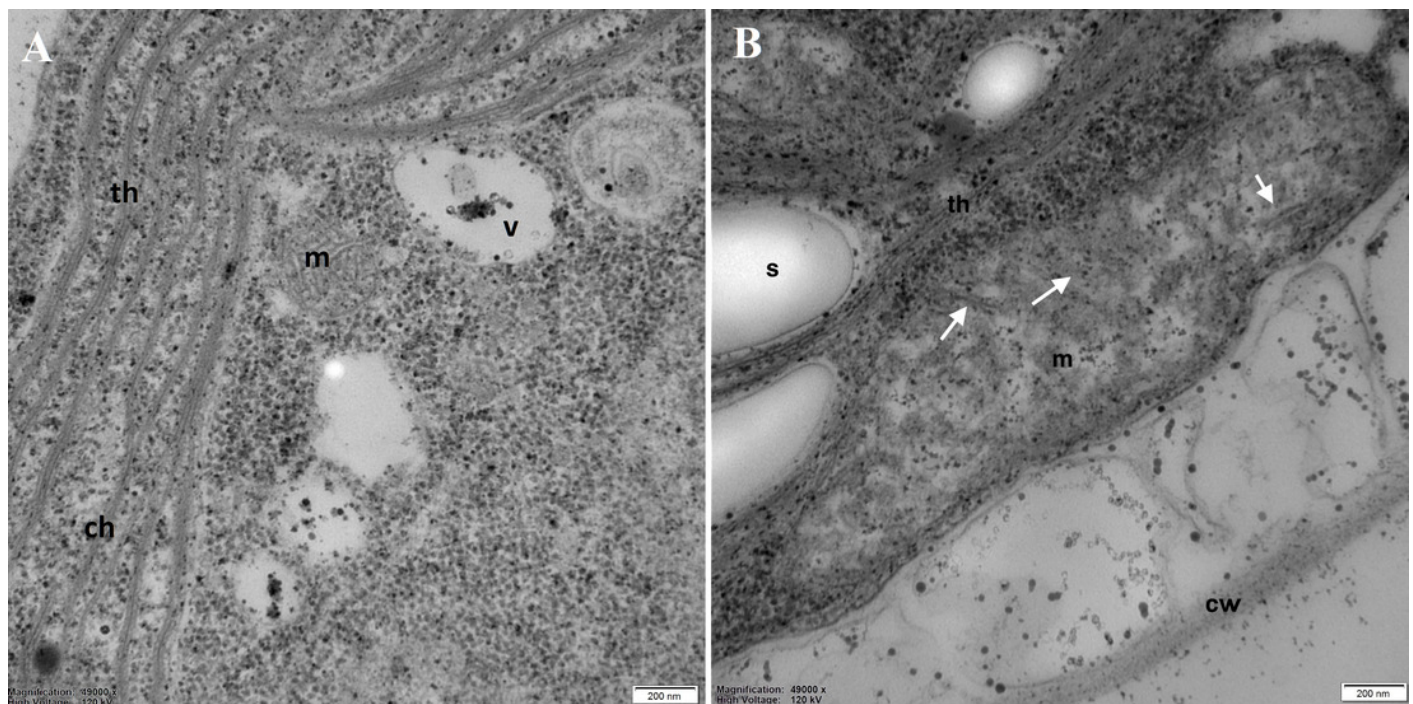
Figure 7

Discriminant analysis of MMP, cell volume, and oxygen consumption in *Chlamydomonas reinhardtii* control cells and DCF-treated cells, incubated with ETC-blockers or non-blocked.

Cells were sampled at 6th h of the light phase of the cell cycle. KCN = potassium cyanide-treated cells; SHAM = salicylhydroxamic acid-treated cells; DCF = diclofenac-treated cells. The ellipses on the figure show the data distribution with a range of coefficient of 1.4.